Journal of
Synchrotron
Radiation

ISSN 0909-0495

Received 15 October 2004
Accepted 28 April 2005

Microfluidics of soft matter investigated by small-angle X-ray scattering

Alexander Otten,[a] Sarah Köster,[a,b] Bernd Struth,[c] Anatoly Snigirev[c] and Thomas Pfohl[a,b]*

[a]Applied Physics Department, University of Ulm, Albert-Einstein-Allee 11, 89069 Ulm, Germany, [b]Max Planck Institute for Dynamics and Self-Organization, Bunsenstraße 10, 37073 Göttingen, Germany, and [c]European Synchrotron Radiation Facility, 6 rue Horovitz, BP 220, 38043 Grenoble CEDEX, France. E-mail: thomas.pfohl@mpi-sf.mpg.de

The combination of X-ray microdiffraction and microfluidics is used to investigate the dynamic behaviour of soft materials. A microfocused X-ray beam enables the observation of the influence of droplet formation on the nanostructure of a smectic liquid crystal in water. Using a hydrodynamic focusing device, the evolution of the intercalation of DNA into multilamellar membranes can be studied. Owing to the elongational flow at the centre of this device, alignment of the material is induced which allows for an improved structural characterization. Furthermore, the influence of strain applied to these materials can be tested.

Keywords: dynamics of soft matter; alignment; droplet formation; hydrodynamic focusing; DNA cationic membrane complexes.

1. Introduction

Recently, remarkable progress has been achieved in the integration and analysis of chemical and biological processes on the nanolitre scale by using microfluidic handling systems (Beebe *et al.*, 2002; Hansen & Quake, 2003). These microfluidic systems enable the reduction of sample volumes, shorter reaction and analysis times, high throughput and parallel operations on a single microfabricated chip ('lab-on-a-chip'). Furthermore, owing to the interesting physics of fluid flow on the microscale, microfluidics is a powerful tool for the investigation of soft condensed matter and biological systems (Pfohl *et al.*, 2003). Besides fluorescence microscopy and spectroscopy, small-angle X-ray scattering is about to play a prominent role as a powerful characterization technique. In a pioneering experiment, Pollack *et al.* (1999) investigated the compaction of a protein by combining small-angle X-ray scattering with microfluidics. An additional focusing of X-ray beams down to the micrometre scale offers the ability to characterize the influence of microscale confinement on nanoscale structures of soft condensed matter such as biomaterials (Struth *et al.*, 2004).

In this paper we describe two microfluidic experiments on the dynamic behaviour of soft materials, which are investigated by X-ray microdiffraction. The formation of microdroplets of a liquid crystal in water represents an interesting example for studying the influence of microscale confinement on a nanostructure. Furthermore, this is a model system for testing the application of microdiffraction on emulsions-based microreactors for chemical networks (Song *et al.*, 2003; Zheng *et al.*, 2004). In a second experiment, we used a hydrodynamic focusing microdevice (Knight *et al.*, 1998) for the investigation of the intercalation process of DNA into a multilamellar membrane system.

2. Experimental set-up

2.1. Microdiffraction

The small-angle X-ray microdiffraction experiments were conducted at beamline ID10B at the European Synchrotron Radiation Facility (ESRF). The ID10B beamline is a multipurpose high-brilliance undulator beamline for high-resolution X-ray scattering and surface diffraction on solids and liquids (Struth *et al.*, 2004). ID10B provides a clean highly collimated X-ray beam with a flux at the sample of 10^{12} photons s^{-1} mm^{-2} (100 mA at 9 keV) that is ideally suited for surface diffraction studies of high-quality single crystals. The microdiffraction set-up is sketched in Fig. 1. The microfluidic device was mounted onto the ID10B goniometer and the X-ray beam was adjusted by using focusing optics mounted onto a secondary stage for optical elements. Two different focusing optics were used. For the experiments with the liquid-crystalline droplet formation, monochromated X-rays at 8 keV (λ = 1.55 Å) were focused to a beam spot of diameter $\sim$6 µm by a Fresnel phase zone plate (Struth *et al.*, 2004). The Fresnel zone plate was made out of silicon on a silicon membrane of thickness 10 µm, which results in 85% transmission of the plate at 8 keV. In total the zone plate consists of 144 zones. The first zone radius is 14.38 µm and the

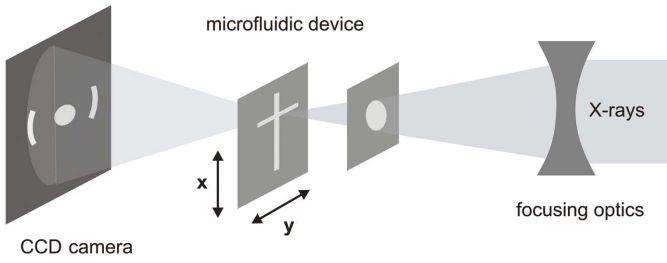

Figure 1
Schematic of the microdiffraction set-up at ESRF beamline ID10B.

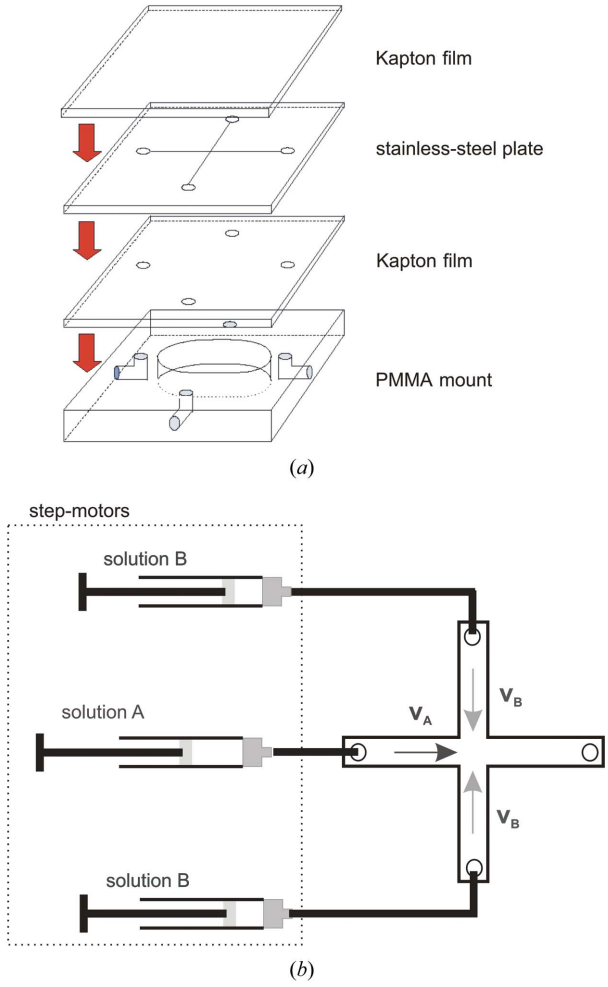

Figure 2
Schematic of (*a*) the design of the microfluidic device and (*b*) the microfluidic pumping system.

last zone width is 0.6 µm. The full aperture of the zone plate is 345 µm (diameter of the active part). At 8 keV the focal distance is 1.33 m and a gain factor of 200 can be obtained. Beryllium compound refractive lenses (Snigirev *et al.*, 1996; Lengeler *et al.*, 2002) were used to focus the X-ray beam down to a spot of diameter ∼20 µm for the investigations on DNA cationic membrane complexes. These compound refractive lenses have a focal distance of ∼1.30 m, and a gain factor of >1000 is achieved. As a detector we used a CCD camera with fluorescent screen and the resultant two-dimensional images of the diffraction patterns covered a q range of 0.02–0.35 Å^{-1}. The smectic layer spacing of the liquid crystal 8CB (4′-*n*-octyl-4-cyanobiphenyl; Sigma-Aldrich) served as calibration. The exposure time of a single image was 120 s using the Fresnel zone plate and 30 s using compound refractive lenses.

2.2. Microfluidic devices

Microfluidic devices for liquid-crystal droplet formation as well as for hydrodynamic focusing and diffusive mixing consist of flow chambers with two crossed rectangular microchannels (Fig. 2*a*). The perpendicularly crossing channels, having a width of 100–150 µm and a depth of 200–300 µm, were spark eroded into stainless steel plates. Top and bottom surfaces of the plates were covered by thin Kapton foils (thickness 20 µm) which had been spin coated with thin poly(dimethylsiloxane) films (thickness <10 µm) and adhered to the steel surfaces to provide a tight cover for the channels. Four holes were punched into the bottom Kapton foils fitting the channel ends of the steel plates. The Kapton–steel–Kapton system was mounted onto a poly(methylmethacrylate) (PMMA) support with corresponding connections to the channel ends. The centre region of the PMMA support was milled out to provide an undisturbed pathway for X-ray beams. The PMMA support was connected to a pumping system by Teflon tubing (Fig. 2*b*). The pumping system utilized three microlitre syringes, one for the main channel and two for the side channels. The step motors of the syringes were controlled by a *LabVIEW* computer interface. The home-built syringe pumps allowed for a continuous pumping of very low flow rates (10^{-9} L s^{-1}). The resulting experimental flow velocities were between ∼100 and ∼15000 µm s^{-1}.

3. Formation of liquid-crystal droplets

Since the mesoscopic structure of the thermotropic liquid crystal 8CB shows a strong influence of geometric constraints (Pfohl *et al.*, 2001), this model system was chosen for our initial microfluidic studies. The rod-shaped 8CB molecules form various liquid-crystalline phases. At temperatures above 313.5 K the material is in an isotropic phase, between 313.5 and 306.5 K in a nematic phase, and below 306.5 K in a smectic A phase. In the smectic A phase the liquid-crystal molecules are organized into stacks of liquid-like layers forming a one-dimensional density wave (Pfohl *et al.*, 2002). The 8CB microdroplets were formed at room temperature in a crossed microchannels device. A schematic illustration of the experimental set-up is shown in Fig. 3. The liquid crystal was pumped into the main channel with a mean flow velocity v_{8CB} of ∼100 µm s^{-1} and the aqueous side streams were pumped with a mean velocity of $v_{H2O} = 10v_{8CB} \simeq 1000$ µm s^{-1}. The droplet formation is achieved by the competition between the resulting shear force and the surface tension of these two immiscible 'liquids'. Owing to the device design, the generated 8CB droplets drain off through the outlet channel. Using an X-ray beam, which was microfocused by a Fresnel zone plate, we were able to measure the two-dimensional diffraction

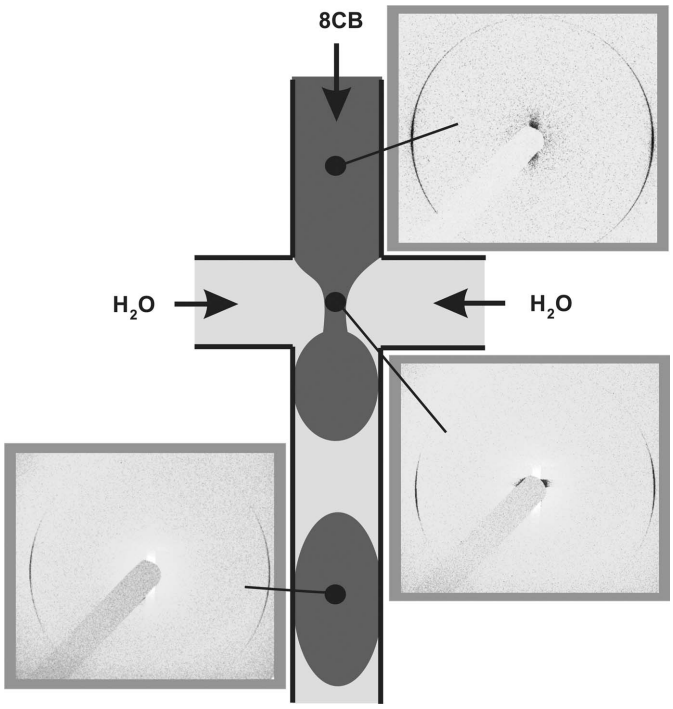

Figure 3
Schematic of the 8CB droplet formation with diffraction patterns observed at three different observation positions along the formation process.

Figure 4
Fluorescence micrographs of the droplet pinch-off taken at the centre of the two crossed microchannels.

pattern of 8CB at different positions of the microfluidic device with a spatial resolution of ∼6 µm. Diffraction patterns of 8CB in the main channel, at the centre of the crossed channel device and in the outlet channel are displayed in Fig. 3. The peak on the two-dimensional diffraction pattern taken in the main channel shows an orientation which corresponds to an alignment of flowing smectic 8CB layers in the flow direction. Reaching the area of the droplet formation in the surrounding aqueous phase, an orientation of the smectic layers in the flow direction still exists, but the azimuthal distribution of the orientation is narrower than before. This diffraction pattern is averaged over several droplet pinch-offs during an exposure time of 120 s. In Fig. 4, fluorescence micrographs of the pinch-off process of 8CB droplets in an aqueous solution of fluorescein are shown. The elongated droplet pinch-off seems to lead to a smaller orientation distribution around the preferential orientation along the flow direction. Moving the observation position towards the outlet channel, the diffraction pattern of 8CB microdroplets can be obtained. The liquid-crystal layers in the droplets have a preferential orientation in the flow direction as well. The diffraction pattern is also averaged over several droplets in the surrounding aqueous phase, which can be seen by the reduced intensity of the peak in comparison with the measurements in the main channel. The ability to characterize the nanostructure of liquid-crystalline droplets establishes the possibility of analysing emulsions-based microreactors for chemical networks (Song *et al.*, 2003) by means of X-ray diffraction. This does not only apply to the formation of crystalline structures (Zheng *et al.*, 2004) but also to much weaker scattering liquid-crystalline materials, as we have shown in this experiment.

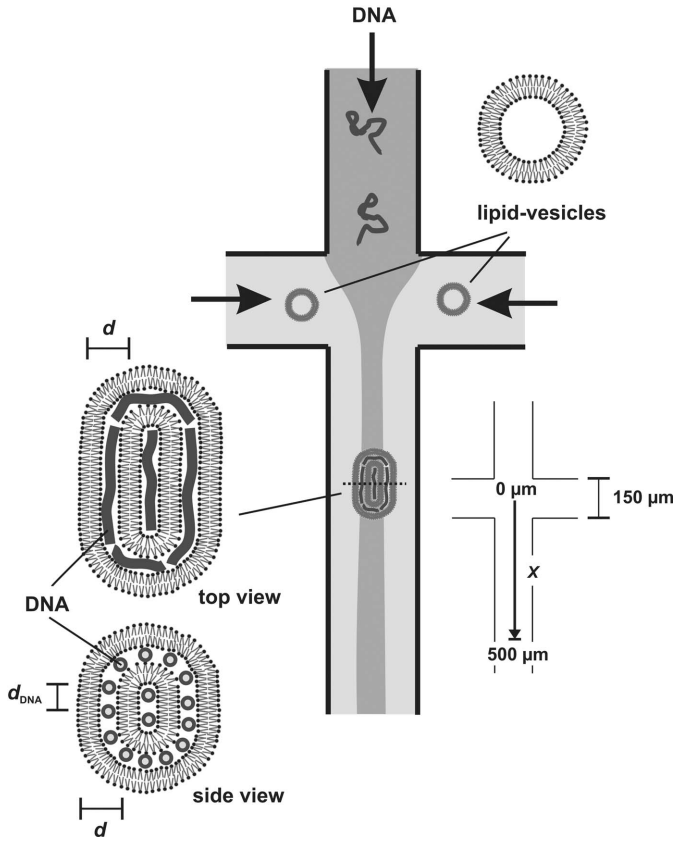

Figure 5
Schematic of the self-assembling of DNA multilamellar membranes in a hydrodynamic focusing and mixing device.

4. DNA intercalation in multilamellar membranes

Using two miscible liquids, the crossed microchannel arrangement allows for hydrodynamic focusing of a liquid stream and at the same time diffusive mixing of the liquids, which opens a wide field of interesting experiments. An incoming liquid flow is hydrodynamically focused by liquid streams of the two side channels (Fig. 5). The width of the focused liquid stream can be adjusted by the ratio of the flow rates of the main channel and side channels. Owing to the laminar flow in microchannel systems, mixing is controlled by diffusion. Reducing the width of the focused liquid stream and

therefore the diffusion length allows for fast mixing and observation of the evolution of interactions between the mixed compounds (Knight *et al.*, 1998; Pollack *et al.*, 1999). The time evolution of the interactions can be spatially separated in steady-state flow.

We used a hydrodynamic focusing device to study the intercalation of DNA into multilamellar cationic lipid layers in combination with an X-ray microdiffraction set-up. The X-ray beam was focused by beryllium compound refractive lenses. Two-dimensional diffraction patterns of the liquid-crystalline materials at different positions within the microfluidic device could be obtained with a spatial resolution of $\sim$20 µm and an exposure time of 30 s. A schematic illustration of the experiment is shown in Fig. 5. DNA cationic membrane systems mimic certain characteristics of natural viruses in their ability to transport DNA across the cell membrane and have been used as synthetically based non-viral carriers of DNA vectors for gene therapy (Rädler *et al.*, 1997; Wong *et al.*, 1998). An aqueous solution of highly polymerized calf thymus DNA (5 mg ml^{-1}; Sigma-Aldrich) in the main channel was pumped with a mean flow velocity $v_{\rm DNA}$ of $\sim$100 µm s^{-1}. An aqueous solution of vesicles (diameter <200 nm) consisting of a 1:1 mixture of the cationic lipid DOTAP (dioleoyl-trimethylammoniumpropane; Avanti Lipids) and the neutral lipid DOPC (dioleoyl-phosphatidylcholine; Sigma-Aldrich) with a total lipid concentration of 25 mg ml^{-1} was added to the side channels with mean flow velocities between $v_{\rm Lipid} = 13v_{\rm DNA}$ and $v_{\rm Lipid} = 130v_{\rm DNA}$. Small-angle X-ray scattering data of the self-assembling of the DNA membranes at different positions x of the mixing and interaction area of the microfluidic device for $v_{\rm Lipid} = 13v_{\rm DNA}$ are shown in Fig. 6. The weak peak at $q \simeq 0.087$ Å^{-1} measured in the centre of the crossed microchannel device ($x = 0$) corresponds to the (001) peak of a layered structure with an interlayer spacing of $d \simeq 72$ Å. Moving the spatial position along the outlet channel down to $x = 100$ µm, the (001) peak becomes stronger and a second peak corresponding to the (002) peak of the multilamellar structure is obtained. Additionally, a weak peak at $q \simeq 0.13$ Å^{-1} appears, which arises from the DNA–DNA correlation in the intercalated layer and corresponds to a DNA interaxial distance $d_{\rm DNA} \simeq 48$ Å (Rädler *et al.*, 1997; Pfohl *et al.*, 2002). This peak becomes stronger when moving the observation position towards larger x, whereas the intensities of the peaks of the multilamellar structure do not increase any more. Note that the used DNA solutions as well as the vesicle solutions do not show any scattering signal in this q range. Interlayer spacing d and DNA interaxial distance $d_{\rm DNA}$ are plotted *versus* observation position x in Fig. 7. The interlayer spacing d is the sum of the membrane thickness $d_{\rm M}$ and the water gap with intercalated DNA layer $d_{\rm W}$ in between two membranes. The interlayer spacing d does not show a dependence on the observation position and an almost constant spacing of $d = 72.6$ Å can be obtained. In comparison, $d_{\rm DNA}$ has a decrease in spacing between $x = 150$ µm and $x = 200$ µm. After this jump, $d_{\rm DNA}$ remains constant achieving a final spacing of $d_{\rm DNA} = 46.5$ Å. Since the different observation positions correspond to different experimental time points, the self-assembling process can be separated in two steps: a faster first one, the formation of the multilamellar complex, and a slightly slower second one, the rearrangement of DNA within the intercalated layers. The obtained spacing $d_{\rm DNA}$ is in good agreement with the data of Rädler *et al.* (1997), whereas d is slightly larger than the data of this reference. This discrepancy may be caused by the different conditions during the complex formation and the X-ray measurements. In our experiment the formation of the multilamellar membranes is controlled by diffusion with a diffusion length on the micrometer scale, whereas in the 'bulk' experiments of Rädler *et al.* (1997) the

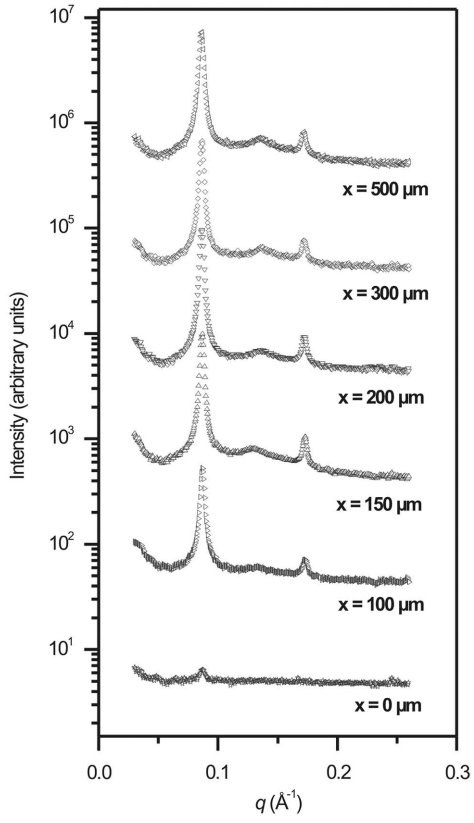

Figure 6
A series of SAXS scans of the self-assembling of the DNA multilamellar membranes at different positions x along the outlet channel for $v_{\rm Lipid}/v_{\rm DNA} \simeq 13$.

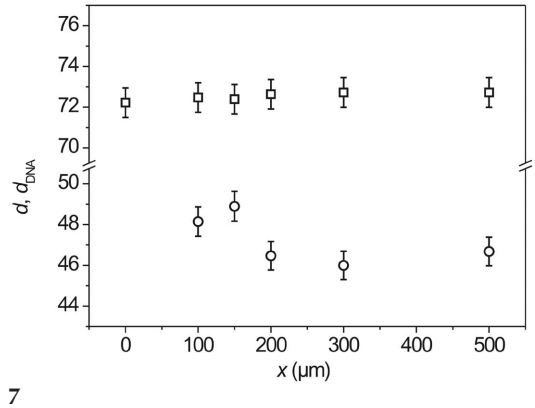

Figure 7
Interlamellar spacing d (squares) and DNA interaxial distance $d_{\rm DNA}$ (circles) plotted as a function of the position x along the outlet channel.

reaction solutions were mixed in a glass capillary by centrifugation.

At the confluence of the main and side channels of the microdevice, the main stream is focused and the fluid elements are accelerated. This elongational flow leads to an orientation and/or deformation of the self-assembling materials. Scans of the azimuthal distribution of the intensity along the ring of the lamellar (001) peak ($q \simeq 0.087$ Å^{-1}) at different x for the flow velocity rates $v_{\rm Lipid}/v_{\rm DNA} \simeq 13$ and $v_{\rm Lipid}/v_{\rm DNA} \simeq 130$ are shown in Fig. 8. For both flow rates a strong orientation of multilamellar membranes along the flow direction (azimuthal angle of maximal intensity $\chi_{\rm max} \simeq 90^\circ$ and $\chi_{\rm max} \simeq 270^\circ$) can be obtained at $x = 100$ µm. At this position, the multilamellar structure (liposomes) experiences a deformation with a preferential orientation in the flow direction (see also schematic illustration in Fig. 5). Moving downstream to the position $x = 500$ µm, the azimuthal intensities of different flow rates show a differing behaviour. For a flow rate of $v_{\rm Lipid}/v_{\rm DNA} \simeq 13$, four local maxima at $\chi_{\rm max} \simeq 90, 180, 270$ and 360° corresponding to a preferential orientation of the multilamellar membranes parallel as well as perpendicular to the flow direction can be obtained. No further acceleration occurs at this position of the microfluidic device and the multilamellar liposomes relax after the induced strain at the confluence of the main and side channels. The relaxed liposomes have an interesting shape consisting of two large multilamellar regions of perpendicular orientation. For a flow rate of $v_{\rm Lipid}/v_{\rm DNA} \simeq 130$ an orientation in flow direction ($\chi_{\rm max} \simeq 90, 270^\circ$) exists at $x = 500$ µm as well. In comparison with the experiment with the lower flow rate, the maximum strain rate and the flow velocity are an order of magnitude larger in this case. Therefore, a relaxation from the more oriented state at $x = 100$ µm has just started, which can be seen in the slightly increased intensity between the two maxima.

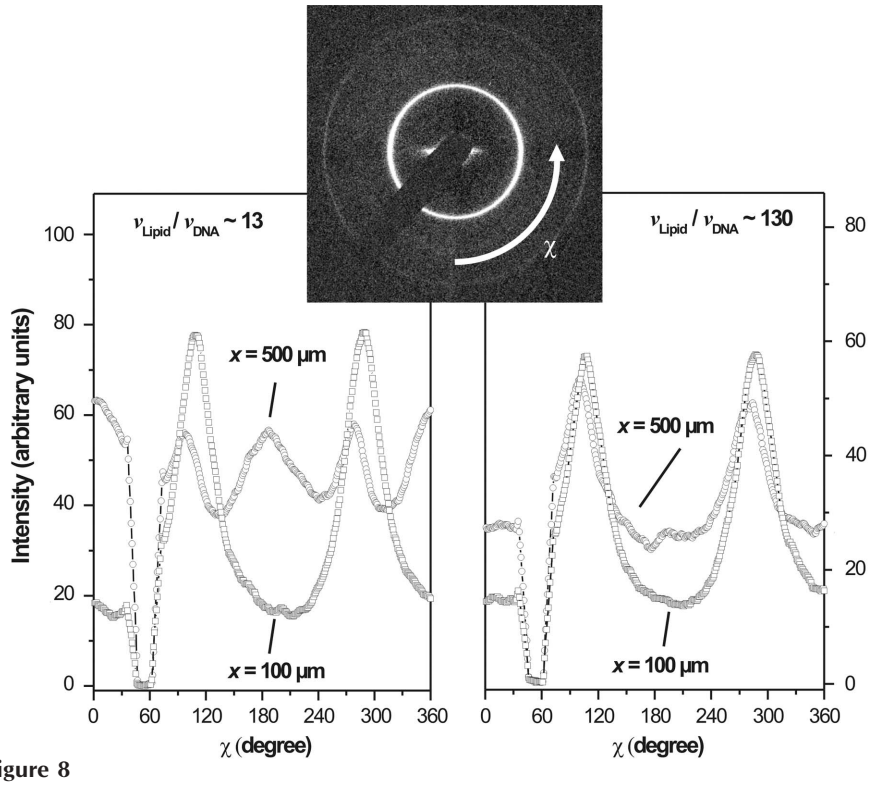

Figure 8
Intensity modulation along the ring of the first peak of the lamellar structure (scans of the azimuth angle χ) at different x for the flow velocity rates $v_{\rm Lipid}/v_{\rm DNA} \simeq 13$ and $v_{\rm Lipid}/v_{\rm DNA} \simeq 130$.

To summarize, microfluidic hydrodynamic focusing and mixing devices offer the ability to study the evolution of the intercalation of DNA into multilamellar membranes by means of X-ray microdiffraction. The induced alignment of the self-assembled structures leads to an improved characterization of these soft materials and additionally the effect of hydrodynamic strain on these materials can be tested.

5. Outlook

Microfluidics used as a tool for studies of soft (biological) materials has an outstanding potential, since these investigations benefit from the physics of the microscale. Combining this technique with microdiffraction and nanodiffraction, novel studies on the dynamics of soft matter in specific consideration of the molecular structure can be performed. More sophisticated control and flow designs will facilitate the development of microfluidic devices with increased functionality and a wider range of applicability. This enables new fascinating experiments including studies on fundamental questions of soft matter physics as well as mimicking the formation of biological networks, such as the cytoskeleton and the extracellular matrix.

We gratefully acknowledge useful discussions with Stephan Herminghaus, Rolf Dootz, Dagmar Steinhauser and Oleg Konovalov. We thank Udo Krafft and Rainer Gauggel for their help in developing the microsyringe system, and the machine shop of the University of Ulm for spark eroding of the steel plates. This work was supported by the DFG within the Emmy-Noether-Programme (DFG 375/2).

References

Beebe, D. J., Mensing, G. A. & Walker, G. M. (2002). *Annu. Rev. Biomed. Eng.* **4**, 261–286.
Hansen, C. & Quake, S. R. (2003). *Curr. Opin. Struct. Biol.* **13**, 538–544.
Knight, J. B., Vishwanath, A., Brody, J. P. & Austin, R. H. (1998). *Phys. Rev. Lett.* **80**, 3863–3866.
Lengeler, B., Schroer, C. G., Benner, B., Gerhardus, A., Günzler, T. F., Kuhlmann, M., Meyer, J. & Zimprich, C. (2002). *J. Synchrotron Rad.* **9**, 119–124.

Pfohl, T., Kim, J. H., Yasa, M., Miller, H. P., Wong, G. C. L., Bringezu, F., Wen, Z., Wilson, L., Li, Y., Kim, M. W. & Safinya, C. R. (2001). *Langmuir*, **17**, 5343–5351.
Pfohl, T., Li, Y., Kim, J. H., Wen, Z., Wong, G. C. L., Kim, M. W., Koltover, I. & Safinya, C. R. (2002). *Colloids Surf. A*, **198**, 613–623.
Pfohl, T., Mugele, F., Seemann, R. & Herminghaus, S. (2003). *Chem. Phys. Chem.* **4**, 1291–1298.
Pollack, L., Tate, M. W., Darnton, N. C., Knight, J. B., Gruner, S. M., Eaton, W. A. & Austin, R. (1999). *Proc. Natl. Acad. Sci. USA*, **96**, 10115–10117.
Rädler, J. O., Koltover, I., Salditt, T. & Safinya, C. R. (1997). *Science*, **275**, 810–814.
Snigirev, A., Kohn, V., Snigireva, I. & Lengeler, B. (1996). *Nature (London)*, **384**, 49–51.
Song, H., Tice, J. D. & Ismagilov, R. F. (2003). *Angew. Chem.* **115**, 792–796; *Angew. Chem. Int. Ed.* **42**, 768–772.
Struth, B., Snigirev, A., Konovalov, O., Otten, A., Gauggel, R. & Pfohl, T. (2004). *SRI 2003 Proceedings*, *AIP Conference Proceedings 705*, pp. 804–807. Melville, NY: AIP.
Wong, G. C. L., Li, Y., Koltover, I., Safinya, C. R., Cai, Z. & Yun, W. (1998). *Appl. Phys. Lett.* **73**, 2042–2044.
Zheng, B., Tice, J. D., Roach, L. S. & Ismagilov, R. F. (2004). *Angew. Chem.* **116**, 2562–2565; *Angew. Chem. Int. Ed.* **43**, 2508–2511.